Quarterly Journal of the Royal Meteorological Society *Q. J. R. Meteorol. Soc.* 140: 2515–2526, October 2014 B DOI:10.1002/qj.2316

RMetS
Royal Meteorological Society

The roles of diurnal forcing and large-scale moisture transport for initiating rain over northwest Australia in a GCM

D. Ackerley,[a]* G. Berry,[a] C. Jakob[b] and M. J. Reeder[a]

[a]*Monash Weather and Climate, School of Mathematical Sciences, Monash University, Clayton, Australia*
[b]*ARC Centre of Excellence for Climate System Science, School of Mathematical Sciences, Monash University, Clayton, Australia*

*Correspondence to: D. Ackerley, Monash Weather and Climate, Monash University, Clayton, Victoria 3800, Australia.
E-mail: duncan.ackerley@monash.edu

The representation of rainfall, and in particular its diurnal cycle, is generally poor in general circulation models (GCMs). Nonetheless, studies make use of GCMs in future climate projections in regions where precipitation has a strong diurnal cycle. In this study we evaluate whether one GCM (ACCESS1.3) can represent the rainfall in such a region (Australia) where the diurnal cycle of rainfall is produced as a result of both the destabilisation of the boundary layer (convection) and a larger-scale reorganisation of the low-level flow, the latter of which may be resolved by a GCM. In northern and eastern Australia, where the diurnal cycle of rainfall is controlled by convective processes, the GCM produces rain 3 to 6 h too early in the day. Nevertheless, the model represents the continental-scale reorganisation of the low-level circulation that results from the diurnal cycle of surface heating and cooling. A nocturnal low-level jet forms over the western half of the continent with strong convergence at the jet exit, which initiates rain overnight in the continental northwest, in agreement with previous work. The model also captures the change in the air-flow direction, from a southeasterly to a northeasterly, responsible for bringing the necessary moisture for precipitation to occur. Thus, while the model may have a tendency to initiate convection too early, it is able to represent the larger-scale nocturnal reorganisation of the flow and the associated rainfall.

Key Words: rainfall; northwest Australia; diurnal cycle; general circulation model; ACCESS1.3

Received 12 September 2013; Revised 8 November 2013; Accepted 6 December 2013; Published online in Wiley Online Library 21 March 2014

1. Introduction

Although there is a pronounced diurnal cycle to precipitation throughout much of the Tropics and Subtropics, the timing of the peak rainfall varies considerably depending on geographic location (Dai *et al.*, 2007). Relative to the local solar time, rainfall maxima tend to occur in the late afternoon over land and in the early hours of the morning over the ocean (Yang and Smith, 2006). Nevertheless, rainfall over the land is not restricted to the late afternoon and may occur overnight, particularly where there is complex surface topography such as the Air Mountains in North Africa (Mohr, 2004), the Himalaya in India (Basu, 2007), the Tibetan Plateau in Southeast Asia (Yuan *et al.*, 2012), the islands of the Maritime Continent (Mori *et al.*, 2004), the Andes in South America (Betts *et al.*, 2002; Poveda *et al.*, 2005) and the Great Dividing Range in Australia (Keenan and Carbone, 2008).

Despite the strength of the diurnal cycle in rainfall and a reasonably good understanding of the physics driving it (Yang and Smith, 2006), general circulation models (GCMs) represent the diurnal cycle poorly as they generally precipitate too early in the day (Yang and Slingo, 2001; Dai, 2006; Dirnmeyer *et al.*, 2012) and therefore tend to underestimate precipitation in the late afternoon and evening. These errors are caused by the premature and rapid development of deep convection following surface solar heating (Betts and Jakob, 2002a,b; Neale and Slingo, 2003; Stratton and Stirling, 2011). Regions where the circulation and precipitation are driven by the local convective processes (such as a destabilisation of the boundary layer) are therefore unlikely to be represented well by GCMs. This study focuses on rainfall over the Australian continent during the summer where such localised convective systems occur (Keenan and Carbone, 2008).

In inland northwest Australia, a nocturnal low-level jet forms in austral summer (Allen, 1980; Brook, 1985). The convergence into the heat low at the exit of the jet is one of the dominant features of the low-level flow over Australia during that season (Racz and Smith, 1999; Spengler *et al.*, 2005; Arnup and Reeder, 2007, 2009). Similar systems have also been identified over West Africa (Parker *et al.*, 2005; Fiedler *et al.*, 2013) and in the mid-west of the United States of America (Dai *et al.*, 1999) where the jet has been shown to trigger nocturnal thunderstorms (Pitchford and London, 1962; Bonner, 1968). The nocturnal, continental-wide re-organisation

of the low-level flow and the associated convergence over Australia is an important, large-scale driver of rainfall (Berry *et al.*, 2011).

However, the nocturnal jet-driven convergence is not the only factor regulating rainfall over northwest Australia. The strong convergence associated with the nocturnal jet occurs both on days with and without rainfall (Berry *et al.*, 2011). It is hypothesised that there must be a change in the atmospheric circulation in order to bring the necessary moisture into northwest Australia for rainfall to occur. This happens through a reorganisation of the low-level flow from the southeast to the northeast with moisture advected from the Coral Sea and the Gulf of Carpentaria into the continental northwest of Australia (Berry *et al.*, 2011). Therefore, in order to represent the rainfall-generating processes accurately, models must (presumably) be able to represent both the change in the wind direction as well as the diurnal cycle of convergence.

The horizontal scales of the nocturnal convergence and the flow regimes responsible for bringing the necessary moisture into northwest Australia may be large enough for a GCM to represent them and therefore reproduce the diurnal cycle of rainfall well in this region. The aims of this study are threefold. The first aim is to determine whether the Australian Community Climate and Earth System Simulator version 1.3 (ACCESS1.3) GCM accurately represents the observed diurnal cycle of the summertime rainfall over northwest Australia. The second aim is to identify whether the diurnal cycles of precipitation and circulation (convergence) covary over the Australian continent. The final aim is to assess whether ACCESS1.3 represents the change in circulation that is responsible for bringing the necessary moisture into northwest Australia for summertime rainfall.

The model, experiments and datasets used in this work are described in section 2. Descriptions of the representation of the rainfall, circulation and moisture transports in ACCESS1.3 (relative to the datasets described in section 2) are given in sections 3–5, respectively. A discussion of the results is given in section 6 to identify whether the rainfall in ACCESS1.3 is related to the circulation and moisture transports in a way comparable with the observervations. The conclusions are given in section 7.

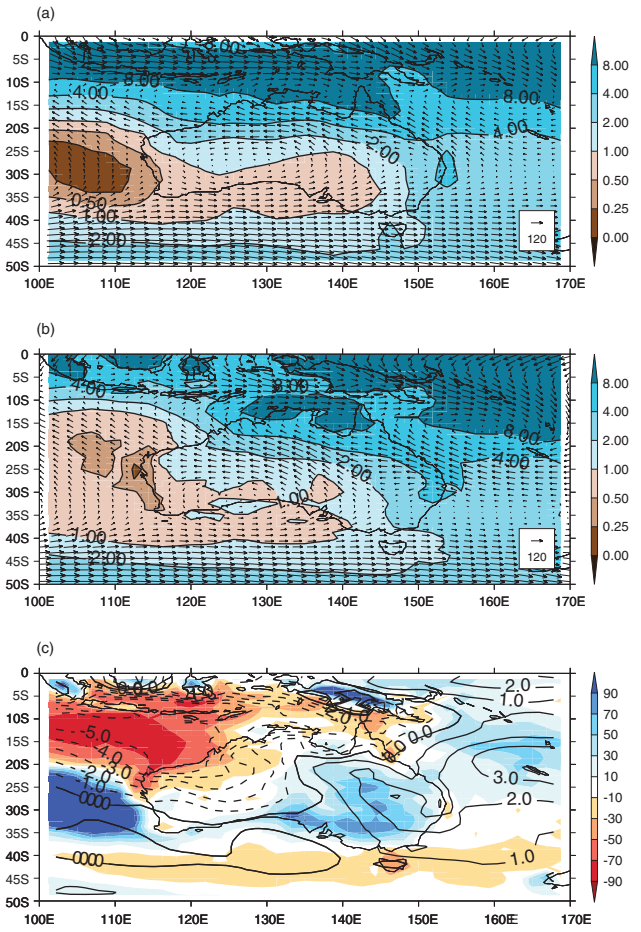

Figure 1. Coloured shading: DJF mean precipitation from (a) CMAP (mm day^{-1}), (b) ACCESS1.3 (mm day^{-1}) and (c) the difference between ACCESS1.3 and CMAP (%). In (a) and (b), arrows show the respective vertically integrated moisture flux (kg m^{-1}s^{-1}) between 925 and 500 hPa. In (c), the solid (dashed) contours represent positive (negative) differences in the column-integrated moisture between ACCESS1.3 and ERA-Interim (kg m^{-2}).

2. Model, experiments and data

2.1. Model and experiments

The atmospheric component of the ACCESS1.3 model is very similar to that in the Met Office Unified Model (MetUM) as described by Hewitt *et al.* (2011). The horizontal resolution of ACCESS1.3 is 1.875° longitude by 1.25° latitude, and there are 38 vertical levels. One of the important differences between the atmospheric components of ACCESS1.3 and the MetUM is that the former uses the Prognostic Cloud Prognostic Condensate (PC2) scheme described in Wilson *et al.* (2008a,b). However, the main difference between the MetUM and ACCESS1.3 is the Commonwealth Science and Industrial Research Organisation (CSIRO) Atmosphere Biosphere Land Exchange (CABLE) land-surface scheme (Kowalczyk *et al.*, 2006), which replaces the Joint UK Land Simulator (JULES; Best *et al.*, 2011, and references therein).

ACCESS1.3 is run from 1978 to 2008 under Atmospheric Model Intercomparison Project (AMIP) conditions (Gates, 1992; Gates *et al.*, 1999, give a description of the AMIP experimental design) with prescribed, monthly sea ice and sea-surface temperatures (SSTs). The SSTs and sea ice are updated using the AMIP-II method (Taylor *et al.*, 2000, give a description) and the model is initialised using the conditions that corresponding to 1 January 1978. The first 23 months, during which time the model spins up, are omitted from the subsequent analyses. The long-term averages referred to in the text are taken over all simulated December–January–February (DJF) seasons from 1979/80 to 2007/08.

2.2. Reanalysis and observational data

The ACCESS1.3 simulations are compared against mean sea level pressure (MSLP), and 925 hPa geopotential height and wind field reanalyses from the European Centre for Medium-Range Weather Forecasts (ERA-Interim; Dee *et al.*, 2011) from 1979/80 to 2007/08. The ERA-Interim reanalysis dataset has a horizontal resolution 1.5° × 1.5°, and 37 vertical levels. These data are bi-linearly interpolated to the grid resolution of ACCESS1.3. The observations assimilated into ERA-Interim are particularly sparse throughout northwest Australia, which may introduce errors in the low-level, reanalysis-derived circulation over land. Nonetheless, there are six radiosonde observation stations across northwest Australia (with data available from 1979 onwards) that were used in ERA-Interim (Uppala *et al.*, 2005; Dee *et al.*, 2011). Also, surface observations are available from numerous Bureau of Meteorology (BoM) sites (Jones *et al.*, 2009, gives the locations of surface stations in Australia), which, in combination with the upper-air soundings, should constrain the reanalyses.

Climatologies of rainfall in the Australasian region are calculated from the Climate Prediction Centre (CPC) Merged Analysis of Precipitation (CMAP) data (Xie and Arkin, 1997). CMAP uses a combination of model, satellite and rain-gauge estimates of rainfall to provide a best estimate of the monthly rainfall totals. Rainfall data are available from 1979 to 2009 at a resolution of 2.5° × 2.5°, which are interpolated to match the grid resolution of ACCESS1.3. CMAP data are averaged over all austral summers between 1979/80 and 2007/08 for comparison with the ACCESS1.3 mean rainfall over the same period.

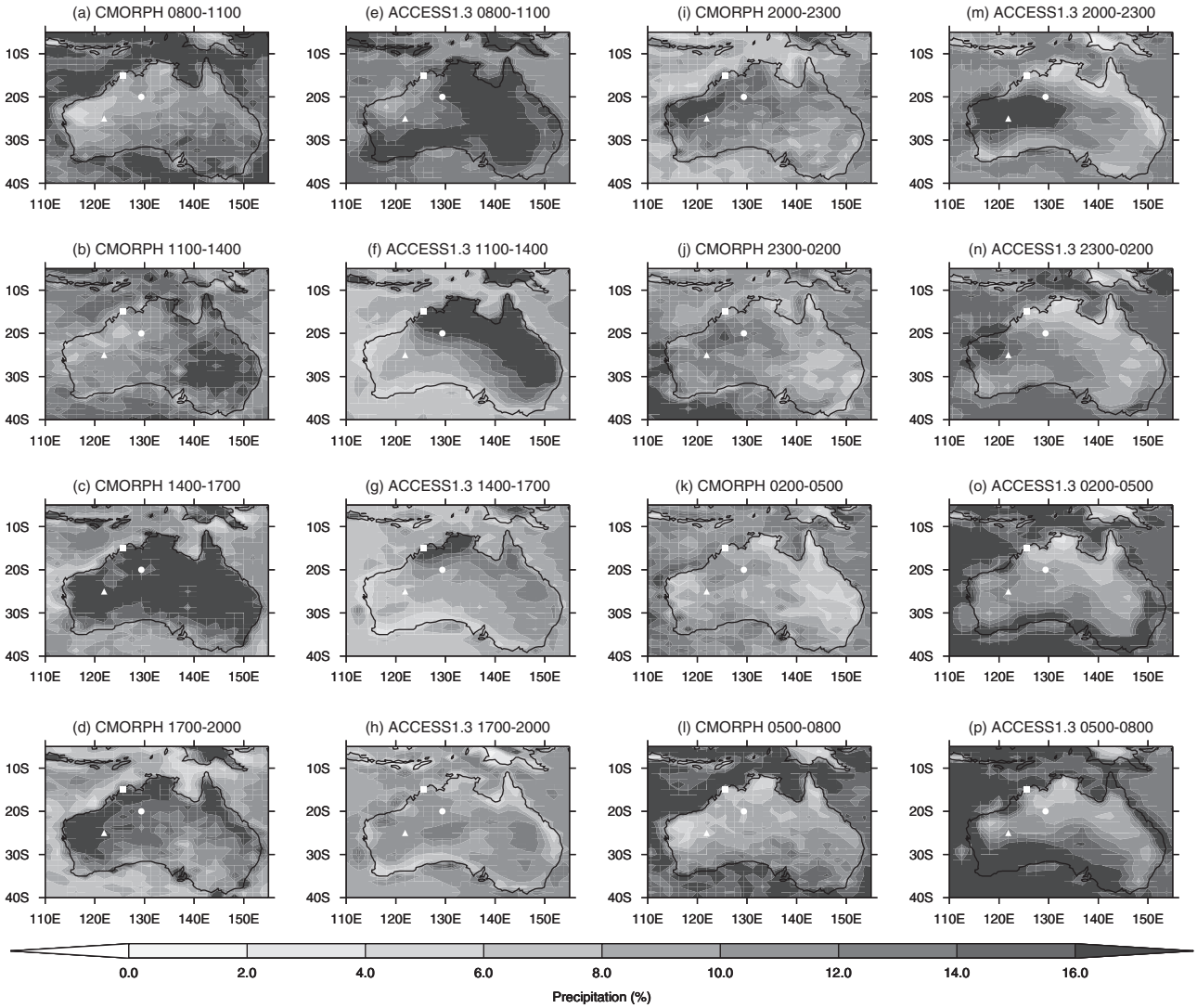

Figure 2. The relative contribution of 3 h rainfall to the daily rainfall (%; days without rainfall are excluded) derived from CMORPH for (a) 0800–1100 AWST, (b) 1100–1400 AWST, (c) 1400–1700 AWST, (d) 1700–2000 AWST, (i) 2000–2300 AWST, (j) 2300–0200 AWST, (k) 0200–0500 AWST and (l) 0500–0800 AWST. (e)–(h) and (m)–(p) show corresponding times and rainfall analysis for ACCESS1.3 (1979/80 to 2007/08). The square, circle and triangle denote Mitchell Plateau, Rabbit Flat and a point within the nocturnal rainfall peak in ACCESS1.3, respectively.

Although CMAP is useful for long-term climatological averages, it does not provide information on the diurnal cycle of precipitation. For this reason, rainfall rates are taken from the Climate Prediction Center morphing (CMORPH) method dataset (Joyce *et al.*, 2004). The CMORPH rainfall data are available as 3 h accumulations at $0.25^\circ \times 0.25^\circ$ resolution between 60°N and 60°S. These data are then re-gridded to the resolution of ACCESS1.3 and used to evaluate the capability of the model to represent the diurnal cycle of rainfall over the Australian continent. Despite the 3 h time resolution of the CMORPH rainfall, the satellite-derived precipitation maximum corresponds with the maximum in deep convective precipitation (cold cloud tops and large hydrometeors), which may be delayed relative to the surface observations that include earlier rainfall from shallower clouds (Dai *et al.*, 2007). As a consequence, we make use of hourly pluviograph rainfall accumulations (provided by the BoM) at Mitchell Plateau and Rabbit Flat (denoted by a square and a circle, respectively, in Figure 2) to validate the diurnal cycle of rainfall in both CMORPH and ACCESS1.3 at those stations. The pluviograph records extend from 1989 to 2006 at Mitchell Plateau and Rabbit Flat.

Following Berry *et al.* (2011), composites of the circulation and geopotential height are derived from 'dry' and 'wet' days in ACCESS1.3 to identify the changes in circulation that lead to the initiation of rain. Only the first day of a rainfall event is used in constructing the composites so that the conditions necessary for the initiation of the rain can be isolated (to some degree) from the atmospheric response to that rainfall. The days with rainfalls less than or equal to 0.2 mm day^{-1} and greater than 0.0 mm day^{-1} are recorded as 'trace' values by the BoM and are not regarded as rain days. Days with rainfall less than or equal to 0.2 mm will therefore be considered as dry days with wet days defined as days where the daily rainfall total exceeds 0.2 mm. The flow regimes in which rain is initiated over northwest Australia in ACCESS1.3 are identified and compared with the results in Berry *et al.* (2011).

All times in this analysis refer to Australian Western Standard Time (AWST), which is 8 h ahead of Coordinated Universal Time (UTC+8).

3. Rainfall

3.1. Climatological mean

The mean grid-point precipitation for DJF from CMAP and ACCESS1.3 are plotted in Figure 1(a, b), respectively. Overlaid in Figure 1(a, b) are the vertically integrated moisture flux vectors, which will be discussed in section 5. ACCESS1.3 captures the higher rainfall in northern Australia and the reduction in rainfall towards the south and west, along with higher rainfall on the east coast than the west coast (the domain pattern correlation is 0.82).

Despite the strong spatial agreement, the root-mean-squared error (RMSE) over the domain in Figure 1 is approximately 2.5 mm day^{-1} (approximately 58% of the plot-domain average). The differences in precipitation between ACCESS1.3 and CMAP

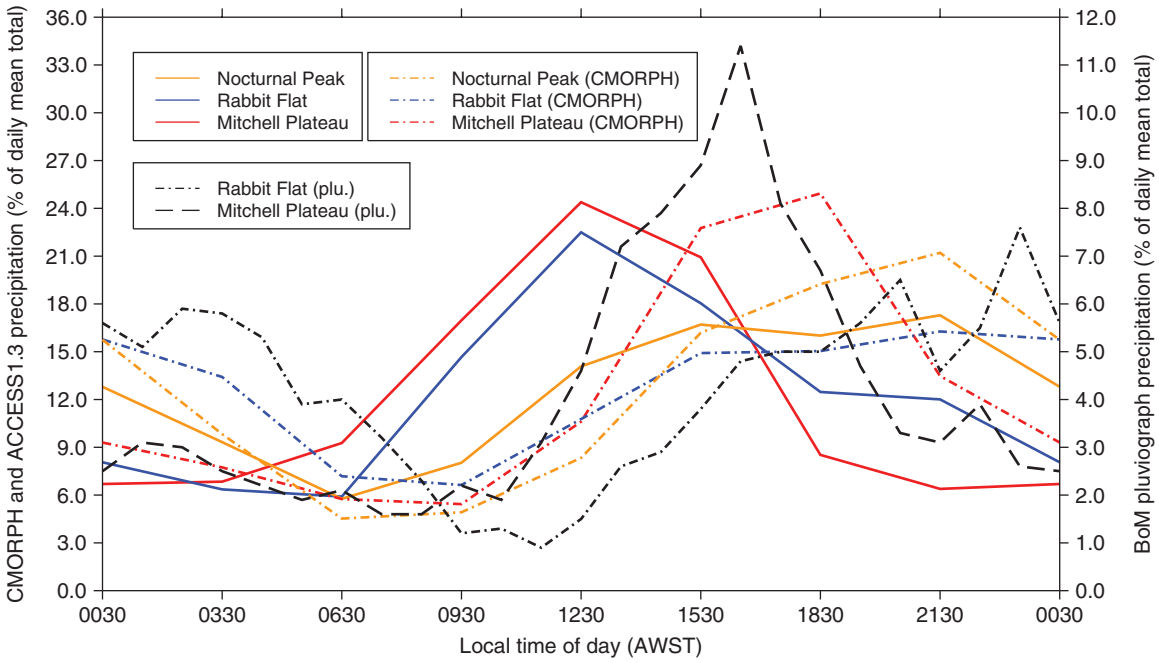

Figure 3. Composite time series of the 3 h percentage contribution to the daily total precipitation in ACCESS1.3 (solid lines) and CMORPH (dot-dashed lines) at Mitchell Plateau (red), Rabbit Flat (blue) and close to the centre of the ACCESS1.3 'Nocturnal Peak' in rainfall (amber) seen in Figure 2. Also plotted are the composite time series of the hourly percentage contribution of rainfall to the daily total taken from the BoM pluviograph data at Mitchell Plateau (black dashed line) and Rabbit Flat (black dot-dashed line). Note the different vertical scales for the pluviograph (right axis) and CMORPH/ACCESS1.3 (left axis) data.

(normalised relative to CMAP) are plotted in Figure 1(c), which shows that the precipitation is too high in the eastern half of Australia and too low towards the northwest. In most areas the magnitude of the difference is less than 50%, including northwest Australia, which has a negative bias of up to −50%. The dry bias over northwest Australia extends into the eastern Indian Ocean and the southwest of the Maritime Continent where it becomes even stronger. Although not shown here, the geographical locations of the positive and negative biases shown in Figure 1(c) are also apparent when the modelled precipitation is compared to two further precipitation datasets (from the Australian Water Availability Project and the Global Precipitation Climatology Project, not shown). This indicates that the differences in Figure 1(c) are primarily caused by deficiencies in the model and not the observational errors.

3.2. *Diurnal cycle*

Composites of the 3 h percentage contribution of rainfall to the daily total accumulation from CMORPH for 1998/99 to 2011/12 are plotted in Figure 2. (Days with zero rainfall are therefore not included in the composites.) The relative contribution is used in order to highlight clearly the timing of rain in areas with both high and low daily accumulations. These composites indicate that rain is initiated in the eastern half of the continent between 1100 and 1400 AWST (Figure 2(b); local time in that region is AWST+2 h) and is followed by an afternoon to evening peak in rainfall between 1400 and 2000 AWST in the continental interior and along the coast (Figure 2(c, d)). There is also evidence for a second inland peak in rainfall during the night in the northwest of the continent (Figure 2(i, j)).

In ACCESS1.3 the majority (greater than 32%) of the daily accumulated rainfall over the northeast of the continent falls between 0800 and 1400 AWST (Figure 2(e, f)), which is approximately 6 h earlier than the CMORPH-derived rainfall (Figure 2(c, d)). Between 1400 and 1700 AWST there is very little precipitation over much of the Australian continent in ACCESS1.3 (Figure 2(g)) when there should be more than 16% of the daily mean rainfall between these times (Figure 2(c)). The model also produces a nocturnal peak in rainfall inland between 2000 and 2300 AWST, although its geographical expanse is larger than the CMORPH rainfall (compare Figure 2(i) and (m)). The nocturnal inland rainfall continues into the early morning in ACCESS1.3 (Figure 2(n, o)), which is consistent with CMORPH (Figure 2(j, k)) but the centre of the maximum between 2300 and 0200 AWST is displaced to the west in the model (compare Figure 2(j) and (n)).

The data from BoM pluviograph sites at Mitchell Plateau (MP, square in Figure 2) and Rabbit Flat (RF, circle in Figure 2) are now used to validate the results from CMORPH and ACCESS1.3 given above. Hourly rainfall data are available at both MP and RF, which means the diurnal cycle from the rain gauges at these points can be compared directly with CMORPH and ACCESS1.3. Time series of the mean diurnal cycle of rainfall from the model and CMORPH at the grid points closest to MP and RF are plotted in Figure 3 alongside the pluviograph records analysed by Berry *et al.* (2011). In the pluviograph time series, the rainfall at MP peaks at approximately 1630 AWST and in CMORPH the peak is between 1700 and 2000 AWST. In contrast, the model rainfall peaks too early (at approximately 1230 AWST). Inland, the peak at RF is close to 2130–0030 AWST in both the pluviograph observations and CMORPH, whereas the model rainfall time series at RF resembles the model time series at MP. However, there is a much smaller secondary peak around 2130 AWST at RF, which suggests that the rainfall at RF in the model displays the characteristics of both rainfall in the late morning/early afternoon and overnight (Figure 3).

The observed transition from the afternoon rainfall at the coast to the nocturnal rainfall inland is not well represented by the model in the vicinity of the pluviograph site at RF as it lies on the boundary between the two regimes (Figure 2(f, m)). A third point is therefore considered (denoted by the triangle in Figure 2) close to the geometric centre of the nocturnal peak in rainfall between 2000 and 2300 AWST in ACCESS1.3 (Figure 2(m)) where the model may be producing rain overnight for the correct physical reasons. This point is referred to as 'Nocturnal Peak' (NP). The composite rainfall time series at the NP point resembles both the RF pluviograph data and the corresponding CMORPH grid point at NP in Figure 3 (compare the amber solid and dot-dashed lines with the black dot-dashed line). The model is therefore able to represent the diurnal cycle of rainfall within the vicinity of the NP point.

Rainfall in northwest Australia is strongly affected by the internal dynamics of the heat low and the transport of moisture

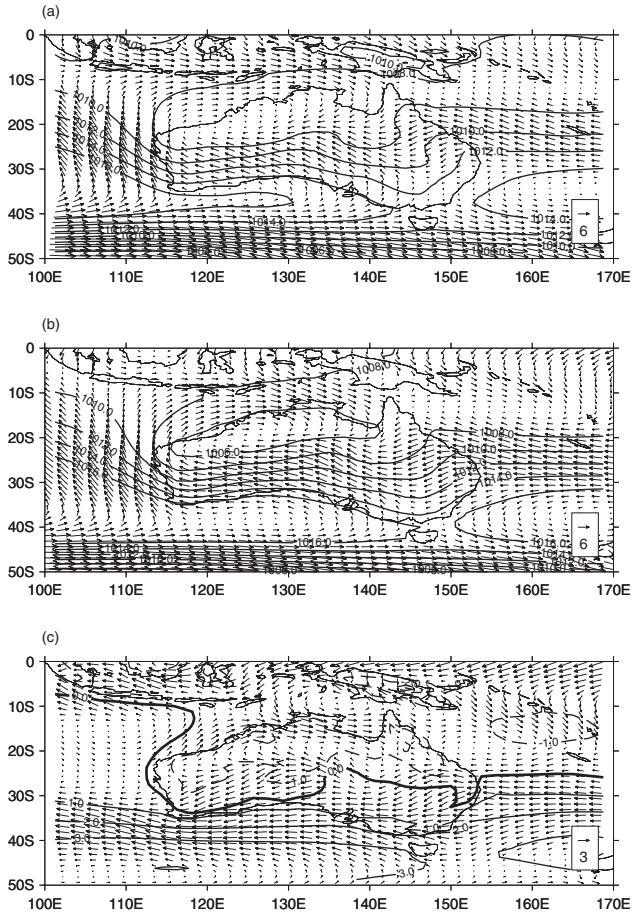

Figure 4. DJF mean, MSLP (hPa) from (a) ERA-Interim reanalyses, (b) ACCESS1.3 and (c) the difference between ACCESS1.3 and ERA-Interim. In (c), positive (negative) MSLP anomalies are solid (dashed). Overlaid are the 925 hPa wind vectors (m s^{-1}; scale given in the bottom right corner of each panel) from (a) ERA-Interim, (b) ACCESS1.3 and (c) ACCESS1.3 minus ERA-Interim.

into the region (as discussed in section 1). The following sections will therefore investigate the representation of each of these ingredients in ACCESS1.3 and compare them to the available observational and reanalysis data.

4. MSLP and circulation

4.1. Climatological mean

The mean MSLP for DJF in the Australian region from the ERA-Interim reanalysis and ACCESS1.3 are shown in Figure 4. The heat low over northern Australia is a prominent feature in both the reanalysis and the model. High pressure centres lie over the southern Indian Ocean (extending into the Great Australian Bight) and the Tasman Sea in both Figure 4(a) and (b). The spatial correlation between the climatological MSLP patterns over the domains given in Figure 4(a) and (b) is approximately 1.0, which indicates that the geographical distributions of higher and lower MSLP are almost identical between the reanalysis and the model.

Despite the high spatial correlation, the MSLP is systematically lower throughout northern Australia and the Maritime Continent (Figure 4(c)) in the model. Consequently, the heat low and monsoon trough are too strong. Conversely, the MSLP is too high to the south of Australia and within the subtropical high pressure systems (Figure 4(c)). The RMSE in the MSLP over the domain used to plot Figure 4 is 1.7 hPa, which implies that model errors in the MSLP of approximately 1–2 hPa are typical throughout this region.

The mean wind vectors in DJF at 925 hPa averaged over 1979/80 to 2007/08 from the ERA-Interim reanalyses, ACCESS1.3 and the difference (ACCESS1.3 minus ERA-Interim) are also plotted in Figure 4(a)–(c). In both the reanalysis and the model, there are easterly winds over most of Australia with westerlies in the southeastern corner of the continent and over the ocean to the south. The difference in the area-averaged zonal wind between the model and the reanalysis (over the domain shown in Figure 4) is -1.17 m s^{-1}, which is caused by the anomalous easterly flow over much of the domain (Figure 4(c)). The anomalous easterlies in the model compared to the reanalysis over the Australian continent are consistent with the stronger south–north MSLP gradient towards the heat low in the model (Figure 4(c)).

4.2. Diurnal cycle

Figure 5(a)–(d) shows the MSLP over Australia from ERA-Interim reanalysis at 0800, 1400, 2000 and 0200 AWST. The heat low deepens throughout the morning and extends over a broad area of northern Australia by 1400 AWST (Figure 5(b)) before becoming shallower overnight with the lowest MSLP located over northwest Australia (Figure 5(d)). Also plotted in Figure 5(a)–(d) are wind vectors and the magnitude of the wind speed at 925 hPa. The circulation associated with the heat low is stronger overnight and is centred at approximately 22°S, 120°E (Figure 5(d)) with north-to-northeasterly flow over much of northern Australia. Another important feature is that the wind turns anticyclonically with time overnight (compare Figure 5(c) and (d)) due to the reduced boundary-layer stress after sunset once the nocturnal boundary layer has formed (Arnup and Reeder, 2009).

ACCESS1.3 displays a similar diurnal variation in the pressure field (Figure 5(e)–(h)); however, the MSLP is lower in the model than in the reanalysis at all times in northern Australia (Figure 5(i)–(l)). The flow around the heat low is similar in the model and the reanalysis at 1400 AWST (compare Figure 5(b) and (f)) with the smallest differences in MSLP and winds (Figure 5(j)). The major differences between the ERA-Interim reanalysis and ACCESS1.3 become apparent later in the day as the circulation centre forms in the west of the continent (Figure 5(k) and (l)). Although the location of the centre of the heat low circulation at 2000 AWST is similar for the reanalysis and the model (Figure 5(c) and (g)), the air flow is more southerly in the model over much of northwest Australia due to the negative MSLP bias (Figure 5(k)). At 0200 AWST, the MSLP is still lower in the model relative to the reanalysis, which causes an anomalous east/southeasterly flow in northwest Australia (Figure 5(l)) .

The ageostrophic wind and convergence at 925 hPa from the ERA-Interim reanalyses and ACCESS1.3 are plotted in Figure 6. The reanalysis shows little ageostrophic flow or convergence early in the morning (Figure 6(a)); however, by 1400 AWST, following surface heating, a strong anticyclonic ageostrophic circulation has formed around the heat low (Figure 6(b)). The ageostrophic flow is the vector difference between the actual wind and the geostrophic wind. As surface solar heating occurs in northwest Australia, turbulent mixing causes the ambient wind speed to become sub-geostrophic, which causes the ageostrophic flow to be negative. As the flow is sub-geostrophic and cyclonic around the heat low, the ageostrophic flow must be anticyclonic (as in Figure 6(b)).

By 2000 AWST, the convergence maximum is centred inland over central and western Australia (Figure 6(c)). The ageostrophic wind turns anticyclonically towards the heat low following the decoupling of the low-level flow from the surface (after the formation of the nocturnal boundary layer), which results in the formation of a nocturnal low-level jet over northwest Australia (as described in Arnup and Reeder, 2007, 2009). The inland convergence at the exit of the low-level jet persists overnight but weakens along with the ageostrophic flow in the early hours of the morning (Figure 6(d)).

ACCESS1.3 displays a similar diurnal cycle to the ERA-Interim reanalysis with weak ageostrophic flow and convergence early in the morning (Figure 6(e)), which strengthens into an anticyclonic ageostrophic circulation with coastal convergence (Figure 6(f)). The centre of the anticyclonic ageostrophic circulation is located

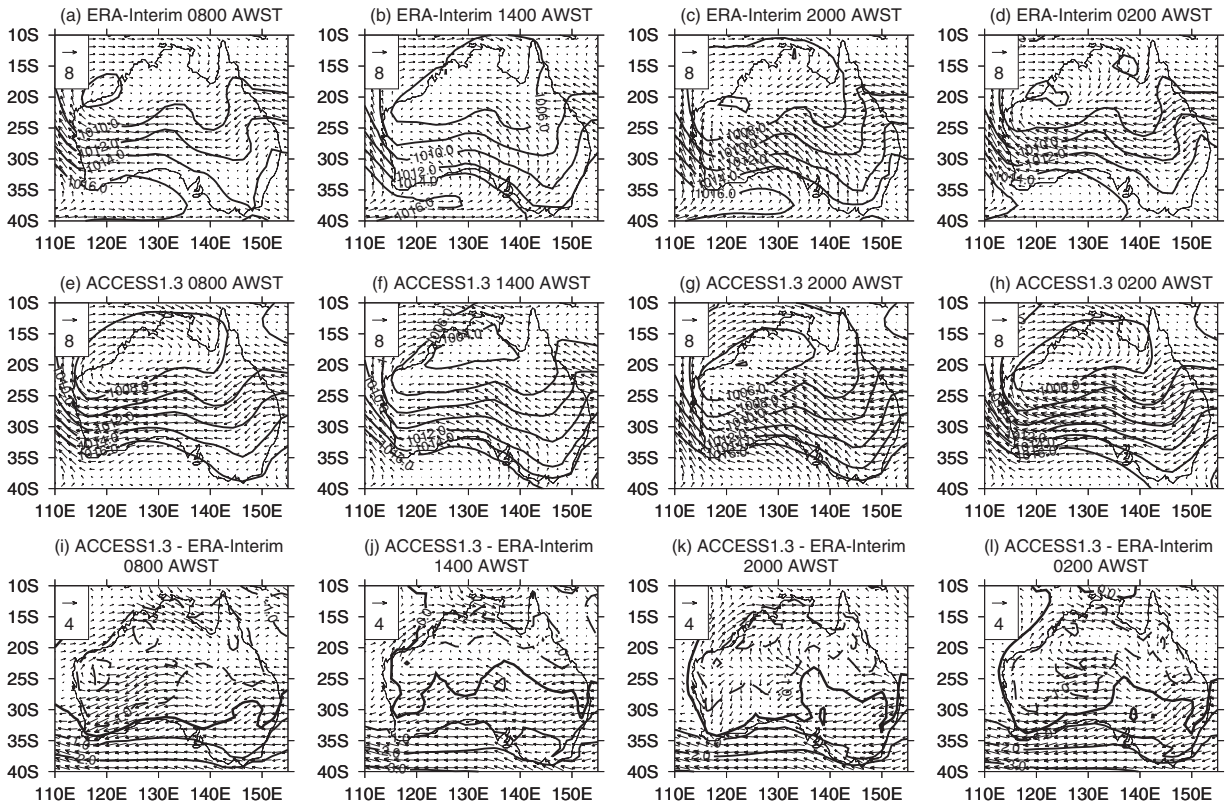

Figure 5. Composited DJF MSLP (hPa) and 925 hPa wind vectors ($m\,s^{-1}$; scale given in the top left corner of each panel) from ERA-Interim reanalyses at (a) 0800 AWST, (b) 1400 AWST, (c) 2000 AWST and (d) 0200 AWST, from ACCESS1.3 at (e) 0800 AWST, (f) 1400 AWST, (g) 2000 AWST and (h) 0200 AWST and the difference between ACCESS1.3 and ERA-Interim at (i) 0800 AWST, (j) 1400 AWST, (k) 2000 AWST and (l) 0200 AWST. Positive (negative) MSLP anomalies in (i)–(l) are solid (dashed).

further north in the model than in the reanalysis (compare Figure 6(b) and (f)). By 2000 AWST, ACCESS1.3 has the nocturnal low-level jet and convergence inland (Figure 6(g)) like the reanalysis; however, the strongest convergence is displaced northward in the model compared to the reanalysis (compare Figure 6(c) and (g)). This northward displacement of the strongest convergence in ACCESS1.3 compared to ERA-Interim reanalysis then persists overnight (compare Figure 6(d) and (h)) and, consequently, the northerly ageostrophic flow remains closer to the north coast in the model.

5. Moisture transport

5.1. Climatological mean

The vectors in Figure 1(a, b) show the time-averaged, vertically integrated moisture flux (F_m, $kg\,m^{-1}s^{-1}$) between 925 and 500 hPa calculated using Eq. (1) (from James, 1994):

$$F_m = \frac{1}{g}\int_{500}^{925} \overline{\mathbf{v}r}\,dp\,. \qquad (1)$$

Here $\mathbf{v}$ is the wind velocity ($m\,s^{-1}$), r is the humidity mixing ratio ($kg\,kg^{-1}$), p is the pressure (Pa) and g is the gravitational acceleration ($9.81\,m\,s^{-2}$). Pressure levels above 500 hPa are not included in the integration (Eq. (1)) as the atmosphere is very dry above this level and the features in Figure 1 do not change when those higher levels are included (not shown).

The ERA-Interim moisture fluxes are easterly over northwest Australia and southeasterly over northeast Australia, which indicates a transport of moisture from the Coral Sea to northern Australia (Figure 1(a)). The moisture flux is more southeasterly in ACCESS1.3 in central and northwest Australia (Figure 1(b)). The difference in the vertically integrated moisture between ACCESS1.3 and the ERA-Interim reanalysis is plotted in Figure 1(c). The vertically integrated moisture in ACCESS1.3 is considerably lower over western Australia (1 to $> 5\,kg\,m^{-2}$ lower), the eastern Indian Ocean and the southwest of the Maritime Continent ($> 5\,kg\,m^{-2}$ lower) than for the reanalysis, which corresponds well with the region of decreased rainfall relative to CMAP (Figure 1(c)).

5.2. Wet versus dry days

Composites for the wet and dry days defined in section 2 at the ACCESS1.3 grid points corresponding with MP, RF, and NP are plotted in Figure 7 to identify the changes in circulation and the associated moisture transports necessary for precipitation.

At MP (square in Figure 7(a)–(c)), wet days occur in ACCESS1.3 when the heat low weakens over northern Australia, which causes a small reduction ($\approx 1\,m\,s^{-1}$) in the westerly wind field at the coast around MP. Apart from the slight increase in geopotential height (≈ 2 m over MP) and weak decrease in the westerly flow, there is little difference between the circulation on wet and dry days at MP.

At RF, a centre of low geopotential height forms to the northwest of the RF grid point, switching the flow from a southeasterly to a northeasterly (Figure 7(d)–(f)) and bringing rain. Similarly, at NP, a change in the wind direction from southeasterly to northeasterly is associated with rainfall (Figure 7(g)–(i)), which is caused by a southwestward displacement of the low geopotential height from 17°S to 22°S (compare Figure 7(g) and (h)).

Berry *et al.* (2011) identified the sources of moisture when it rains at MP and RF with a back-trajectory analysis. The same method is applied to ACCESS1.3 with the trajectories calculated back to 10 days before the rain began (Figure 8). At MP, the air at 925 hPa crosses the ocean to the west of Australia on both wet and dry days (Figure 8(a, b)). On wet days at MP in ACCESS1.3, the air at 850 hPa originates from near the southern Coral Sea whereas on dry days it comes from the eastern Australian continent. Nonetheless, as with the 925 hPa flow (Figure 7(a, b)) the back trajectories are similar for both wet and dry days.

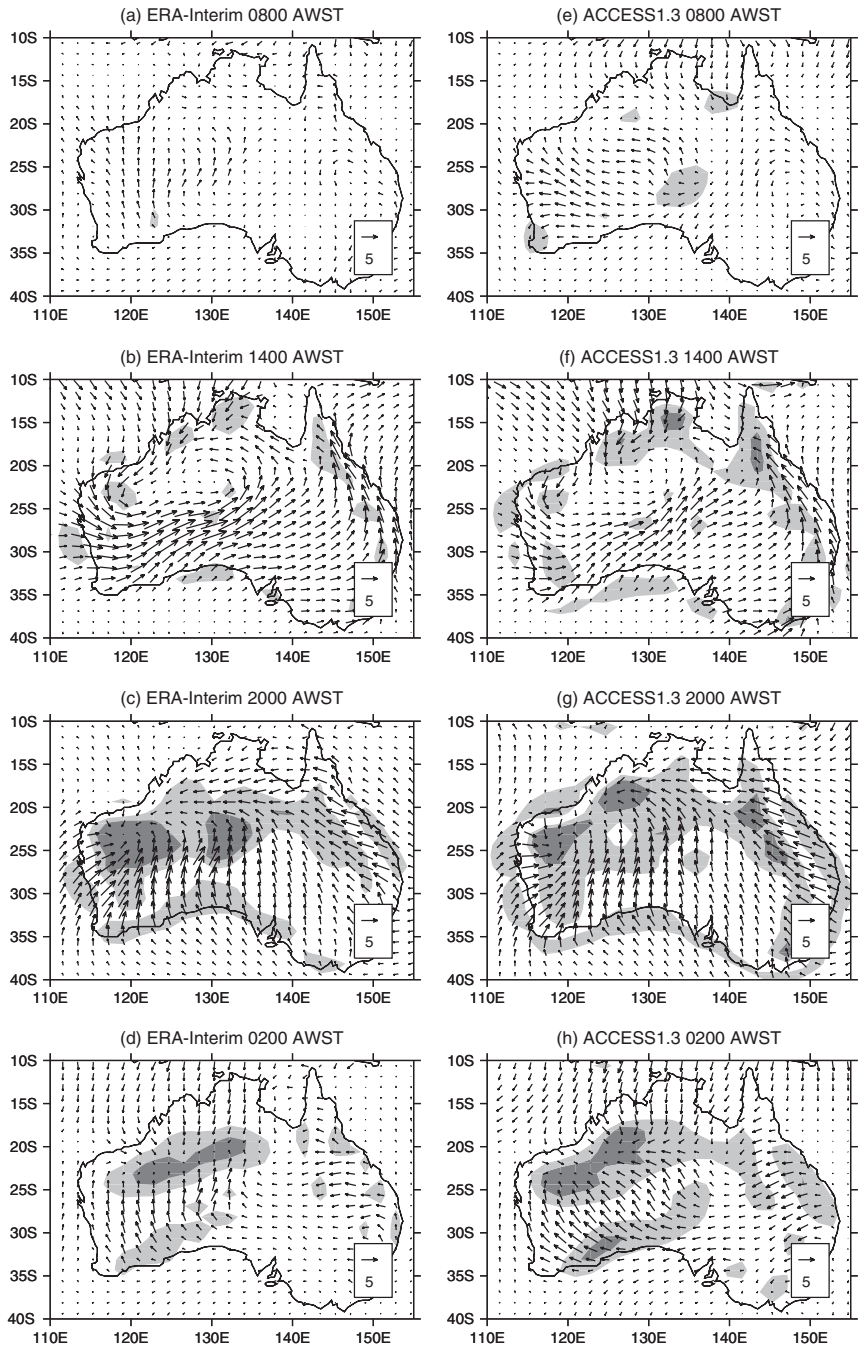

Figure 6. Composited DJF ageostrophic wind vectors ($m\,s^{-1}$; scale given in the bottom right corner of each panel) at 925 hPa for ERA-Interim reanalyses at (a) 0800 AWST, (b) 1400 AWST, (c) 2000 AWST and (d) 0200 AWST and from ACCESS1.3 at (e) 0800 AWST, (f) 1400 AWST, (g) 2000 AWST and (h) 0200 AWST . Shaded areas indicate places where the magnitude of the convergence $\geq|\ 5.0 \times 10^{-6}\,|\,s^{-1}$ (light shading) and $\geq|\ 1.0 \times 10^{-5}\,|\,s^{-1}$ (dark shading).

At RF (Figure 8(c, d)) low-level moisture comes from the ocean to the northwest of Australia and from the Coral Sea (to the east) on wet days. For the dry composites, the air at RF originates from the south Coral Sea at low levels and has to cross the continent before reaching RF.

Back trajectories are also shown for the NP point for the wet and dry composites (Figure 8(e, f)). As with RF, the moisture source is to the north and east of NP at low levels (below 700 hPa) and appears to be the Coral Sea. In the dry composite at NP, the low-level air originates from further south and east (Figure 8(f)).

6. Discussion

6.1. Climatology

The climatological pattern of MSLP is represented well in ACCESS1.3, with the spatial correlation between the ERA-Interim and modelled MSLP approximately 1.0. Nevertheless, there are errors in the modelled MSLP field over northwest Australia. For example, the MSLP is 1–2 hPa too low over northern Australia and 1–3 hPa too high to the south, which results in an anomalously strong easterly flow over the continent (Figure 4(c)). The 1–2 hPa lower MSLP within the vicinity of the heat low in the model is also likely to cause the anomalous south-to-southeasterly flow across northwest Australia. Garcia-Carreras *et al.* (2013) also found similar MSLP biases in the Saharan heat low in the operational version of the MetUM and suggest that the convective parametrisation is responsible for this bias.

There is a high spatial correlation (0.82) between the CMAP precipitation and ACCESS1.3 throughout the Australian region; however, there is disagreement between the model and CMAP. There is a negative precipitation bias over much of the northwest of Australia in ACCESS1.3, which extends into the Indian Ocean towards the southwest of the Maritime Continent and corresponds with a region where the atmospheric moisture contents (below 500 hPa) are from 1 to more than 5 $kg\,m^{-2}$

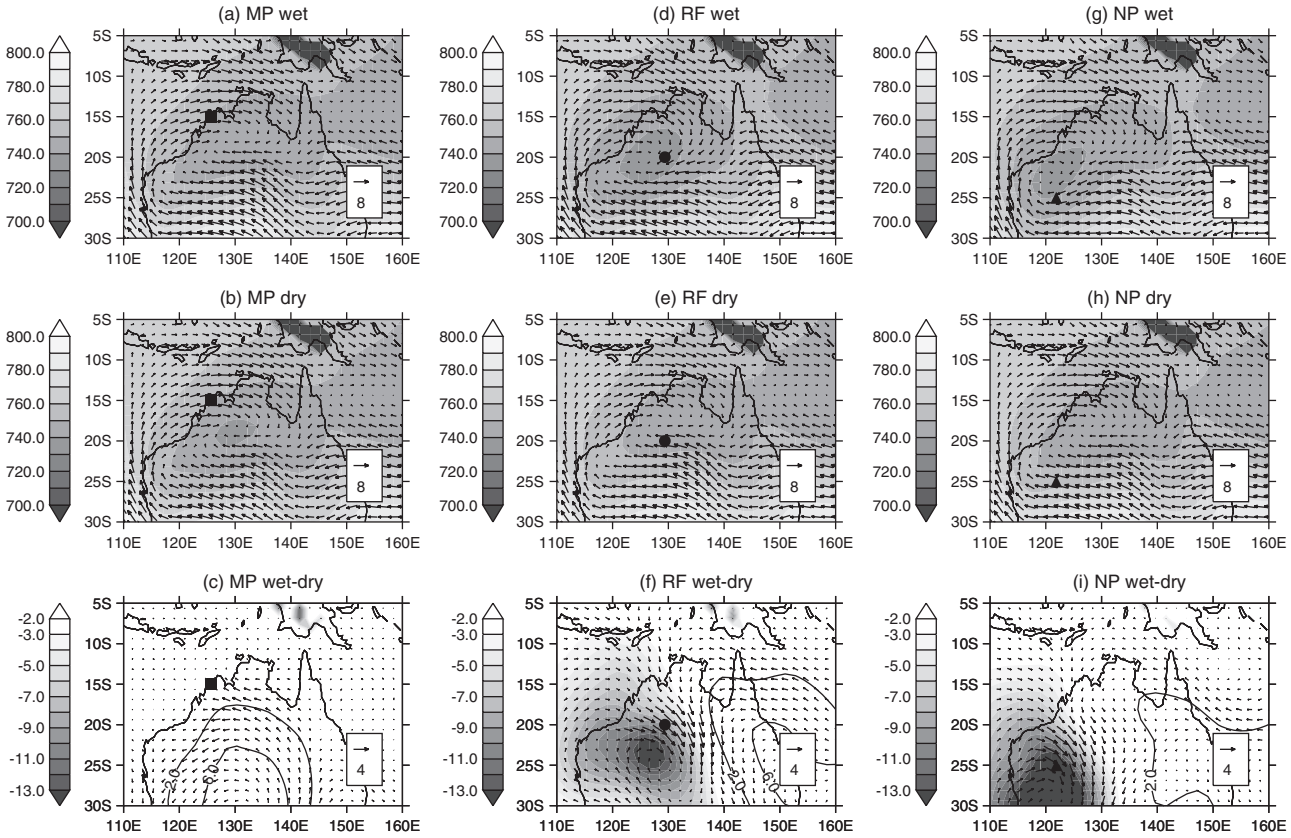

Figure 7. Daily mean geopotential heights (m) and wind vectors (m s^{-1}; scale given in the bottom right corner of each figure) at 925 hPa composited by (a) wet and (b) dry days and (c) wet minus dry days at Mitchell Plateau (square). (d)–(f) and (g)–(i) are as (a)–(c), but the compositing was done at Rabbit Flat (circle) and the 'Nocturnal Peak' (triangle), respectively. In (c), (f) and (i), shaded (solid unshaded) contours indicate negative (positive) geopotential height anomalies.

too low (Figure 1). Neale and Slingo (2003), using an older version of the MetUM, show that an inadequate representation of the Madden–Julian Oscillation, the islands of the Maritime Continent and their associated diurnal cycle (including land–sea breezes) are likely to be responsible for the dry bias in the eastern Indian Ocean. Furthermore, Martin *et al.* (2006) show that the east Indian Ocean dry bias develops within the first 2–5 days of simulations (with a later version of the MetUM), and suggest that the error is related to the convection scheme. As similar dry bias patterns have been found in even later versions of the MetUM (Walters *et al.*, 2011), it is unlikely that the dry bias (Figure 1(c)) had been resolved before the development of ACCESS1.3, which is based on the MetUM. Neale and Slingo (2003) also suggest that the lack of cumulus congestus development over the ocean adjacent to the Maritime Continent in the MetUM reduces the moisture transport from the surface to the mid- to lower troposphere. This is also consistent with the dry bias over the ocean to the north and west of the Australian continent in Figure 1(c). Nonetheless, the dry bias may also be enhanced by the anomalous southeasterly moisture flux across Australia in ACCESS1.3 as airstreams from the southeast are likely to have a more continental trajectory and consequently are drier. The southeasterly moisture flux across Australia in the model is also likely to be responsible for the positive rainfall bias in the southeast (Figures 1(c) and 4(c)).

6.2. *The diurnal cycle and moisture sources*

The diurnal cycle of rainfall over the north and east of the Australian continent differs between the model and the CMORPH dataset (Figure 2). The precipitation is initiated too early in the model with the majority of the rain falling between 0800 and 1400 AWST instead of between 1400 and 2000 AWST, as seen in the CMORPH data. The rainfall in the east of the continent may be partially driven by the stronger (1–2 m s^{-1}) onshore easterlies in ACCESS1.3 compared to the reanalysis between 0800 and 1400 AWST (Figure 5(i, j)); however, the rainfall over the continent in ACCESS1.3 between 0800 and 1400 AWST is not confined to the eastern coastline.

The early rainfall may also be caused by the premature triggering of convection in the model (compared to the real world), which is a known problem within GCMs (Yang and Slingo, 2001; Dai and Trenberth, 2004; Dai, 2006; Stratton and Stirling, 2011) including ACCESS (Brown *et al.*, 2010). Composites of the 3 h percentage contribution of rainfall from deep and mid-level convection (separately) to the daily total accumulation of all convective rain are plotted in Figure 9. (Once again, days with zero rainfall are therefore not included in the composites.) The convection in ACCESS1.3 is defined as 'deep' when air parcels, lifted adiabatically from within the boundary layer, are still buoyant above 2500 m or the 0 °C level (Maidens and Stratton, 2006). Therefore, deep convection is triggered when the boundary layer is destabilised (in this case from solar heating) within a grid box.

The region of precipitation in the eastern half of Australia where more than 16% of the daily rainfall occurs between 0800 and 1100 AWST (Figure 2(a)) and between 1100 and 1400 AWST (Figure 2(b)) corresponds well with the region where more than 12% of the daily convective rainfall is from deep convection between 0800 and 1100 AWST (Figure 9(a)) and more than 16% between 1100 and 1400 AWST (Figure 9(b)). From 1400 to 2000 AWST (Figure 9(c, d)) there is very little rainfall from deep convection over Australia (less than 12% except in the far north) within the model when, in the observations, more than 16% of the rainfall occurs during this time over much of the continent (Figure 2(c, d)). From 1700 to 0800 AWST there is very little rainfall from deep convection over the continent in ACCESS1.3 (less than 4%; Figure 9(d)–(h)) and most of the rainfall from deep convection has finished by 1400 AWST (although there is some mid-level convective precipitation between 1700 and 2000 AWST; Figure 9(l)). The early onset of rainfall in the north and east of the continent therefore appears to be primarily caused by the early triggering of convection within ACCESS1.3.

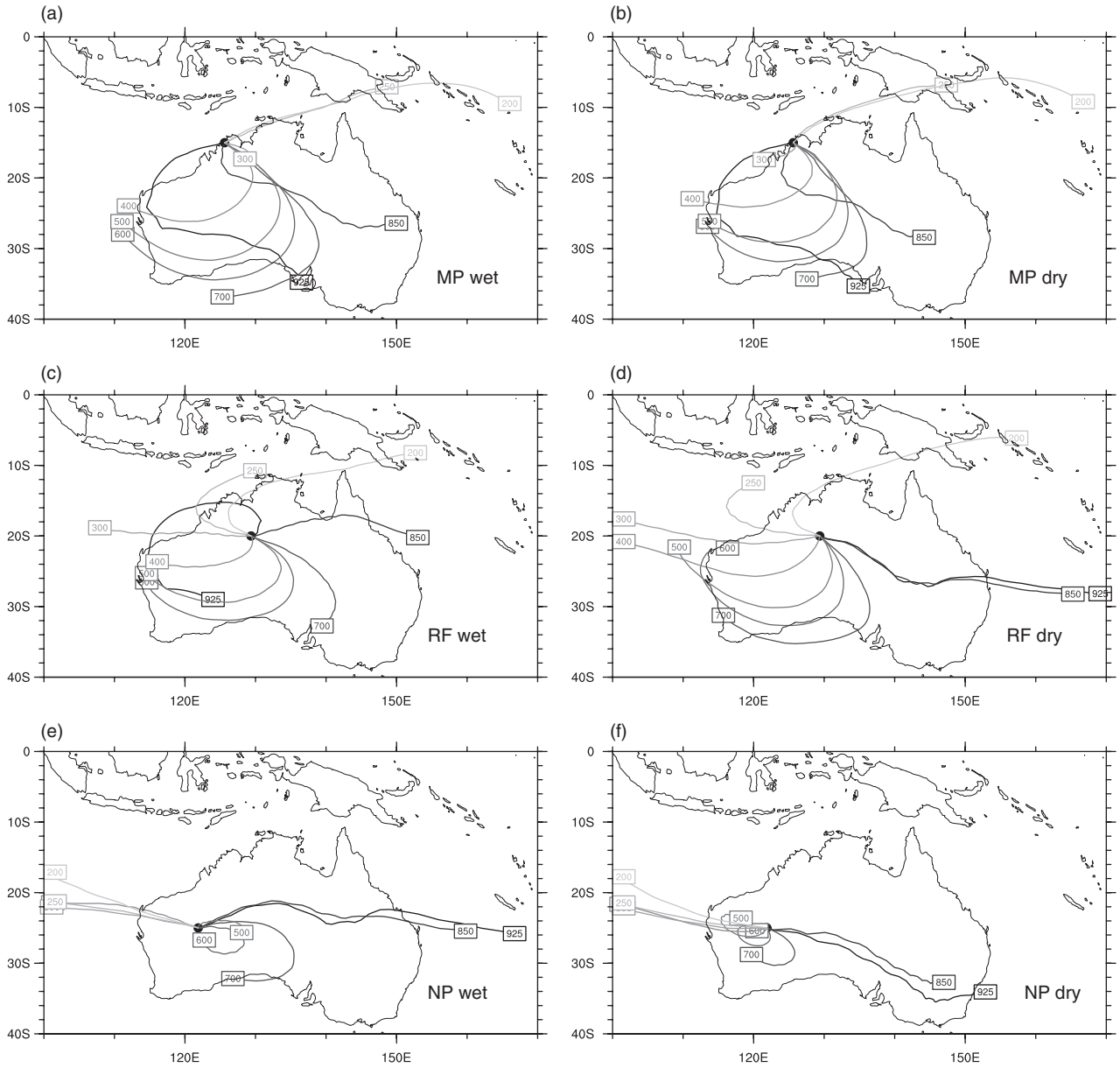

Figure 8. Ten-day back-trajectories along isobaric surfaces (hPa; labelled in the figure) starting at the model (ACCESS1.3) grid point at Mitchell Plateau on (a) wet composites and (b) dry composites. (c, d) and (e, f) are equivalent composites initiated at the Rabbit Flat and 'Nocturnal Peak' grid points, respectively.

Nevertheless, there is a region over northwest Australia where the majority of the precipitation falls between 2000 and 0200 AWST in ACCESS1.3 (Figure 2(m, n)) and CMORPH (Figure 2(i, j)). The increased nocturnal rainfall corresponds with a region of strong convergence in ACCESS1.3 (Figure 6(g, h)) and the ERA-Interim reanalyses (Figure 6(c, d)).

Overnight the low-level air accelerates toward the heat low centre, which results in strong convergence in both the model and the reanalysis (Figure 6) and hence the nocturnal precipitation. Moreover, more than 16% of the convective precipitation between 2000 and 2300 AWST is from mid-level convection (compare Figure 2(m, n) with Figure 9(m, n)), which is defined in ACCESS1.3 as convection that occurs above the boundary layer –in this case above the nocturnal boundary layer. This suggests that ACCESS1.3 can reproduce the continental-wide reorganisation of the flow from day to night and the rainfall associated with it. Nonetheless, there is strong nocturnal convergence in northern Australia (north of 20°S) that is co-located with little overnight precipitation (compare Figure 6(g, h) with Figure 2(m, n)). This area coincides with the location of deep convection earlier in the day (Figure 9(a)–(c)) and suggests that the mid-level convection is largely restricted to the areas where deep convection has not previously removed the instability.

The 925 hPa convergence for wet and dry days at the corresponding ACCESS1.3 grid points used in Figure 3 for MP, RF and NP are plotted in Figure 10. The time series at RF shows that the convergence is stronger during the day and weaker overnight on wet days than on dry days, although the convergence strengthens overnight in both the wet and dry composites. The stronger morning-to-afternoon convergence at RF on wet days agrees well with the majority of the rain falling at this grid point in the late morning or early afternoon. Similarly, at MP and NP the convergence has a tendency to be slightly stronger on wet days and the strongest convergence corresponds well with the largest rainfall during the diurnal cycle (compare Figures 3 and 10). Nevertheless, convergence still occurs at MP, RF and NP on dry days (Figure 10), which is also seen in Berry *et al.* (2011). Therefore, while the local convergence may play a role in triggering convection in the model (as convergence occurs on both wet and dry days), there must be another factor that determines whether or not it rains.

In order for rainfall to occur, there must be sufficient moisture available as no amount of convergence will produce rainfall if the atmosphere is dry. At MP, on the northwest Australian coast, there is little difference between the low-level air flows on wet and dry days in the model (Figures 7 and 8), with weak ($\approx 1\,\mathrm{m\,s^{-1}}$) anomalous southeasterly flow on wet days

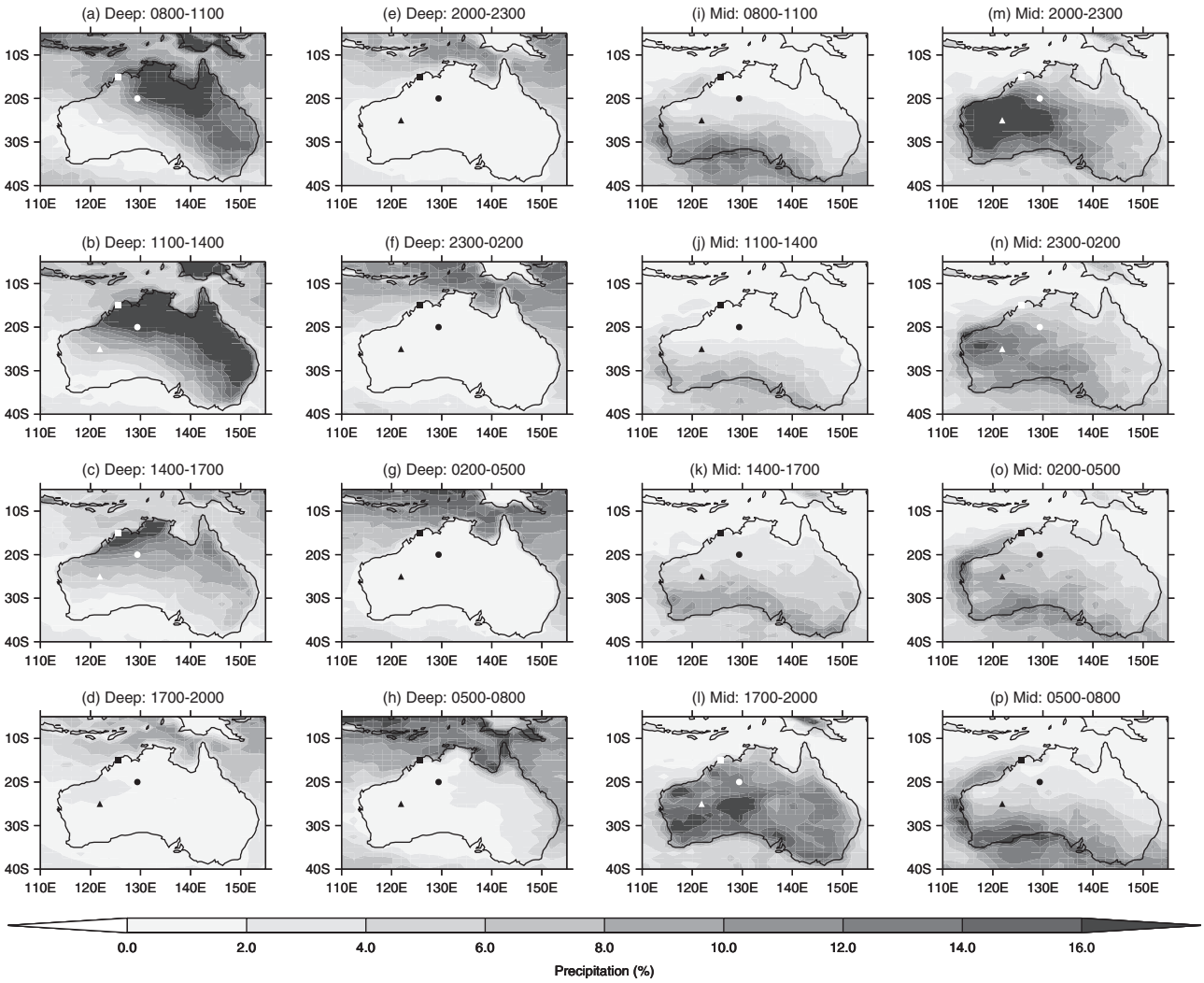

Figure 9. The relative contribution of 3 h rainfall from deep convection to the daily convective rainfall (%; days without convective rainfall are excluded) between (a) 0800 and 1100 AWST, (b) 1100 and 1400 AWST, (c) 1400 and 1700 AWST, (d) 1700 and 2000 AWST, (e) 2000 and 2300 AWST, (f) 2300 and 0200 AWST, (g) 0200 and 0500 AWST and (h) 0500 and 0800 AWST. (i)–(p) are the corresponding relative contributions from mid-level convection. The square, circle and triangle denote Mitchell Plateau, Rabbit Flat and a point within the nocturnal rainfall peak in ACCESS1.3, respectively.

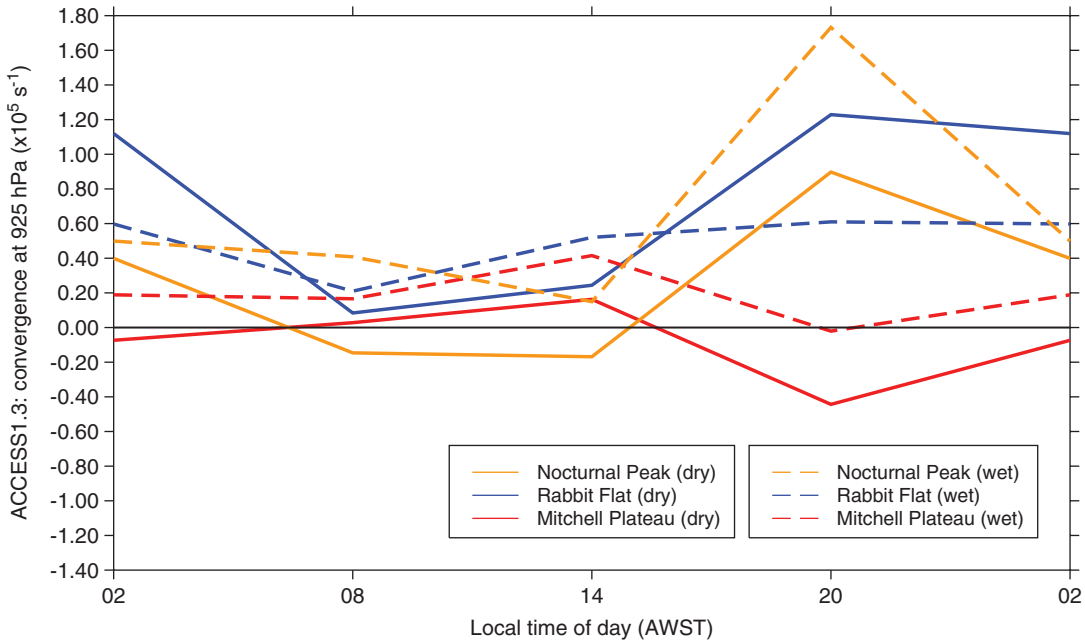

Figure 10. Model-derived horizontal convergence ($\times 10^5$ s^{-1}) at 925 hPa at Mitchell Plateau (red), Rabbit Flat (blue) and the ACCESS1.3 'Nocturnal Peak' (amber) composited on dry (solid) and wet (dashed) days.

(Figure 7(c)). The representation of air flow on wet days in ACCESS1.3 differs from the analysis of Berry *et al.* (2011), which shows that westerly anomalies are associated with rainfall at MP. Therefore the model does not simulate the large-scale circulation correctly on wet days at MP. However, the rainfall at MP appears to be primarily from deep convection (Figure 9(b, c)), which may be driven by local instability (surface solar heating) and moisture availability (in this case from the adjacent ocean). The large-scale atmospheric flow may therefore be less important for precipitation at MP in ACCESS1.3 than in reality (Berry *et al.*, 2011). Also, the anomalous low-level flow in Figure 7(c) may just be the local atmospheric response to the presence of deep convection there. Moreover, rainfall is very sensitive to the representation of air flow at coastal grid points (for example over the Maritime Continent; Neale and Slingo, 2003; Walters *et al.*, 2011) and errors in the circulation over the land/sea interface may also be contributing to the airflow differences between ACCESS1.3 and the Berry *et al.* (2011) study.

At the RF grid point in ACCESS1.3, the low-level wind direction changes from a dry southeasterly on dry days (originating over the continental interior, Figure 7(e)) to a moist northeasterly on wet days (originating from the Coral Sea and the Gulf of Carpentaria, Figure 7(d)) following an anomalous decrease in geopotential height over northwest Australia. This change in air flow agrees well with the analysis of Berry *et al.* (2011). The back trajectories from the wet composite (Figure 8(c)) also indicate that the air has come from the north and east below 850 hPa, which also agrees very well (Berry *et al.*, 2011). Nevertheless, when it does rain at RF in ACCESS1.3, it rains too early in the day (as shown in Figure 3), which is associated with the triggering of the deep convection scheme (Figure 9(a, b)) as the timing of the maximum convergence is after the peak rainfall (compare Figures 3 and 10). However, there is a tendency for more rainfall around 2130 AWST than at 1830 AWST, which corresponds with the timing of the strongest convergence (compare Figures 3 and 10). The RF grid point is on the edge of the region between the deep and mid-level convective regimes (Figure 9) and is likely to be displaying properties of both.

Precipitation at the NP grid point (as with RF) occurs as a result of a change in wind direction from southeasterlies of continental origin on dry days (Figures 7(h) and 8(f)) to northeasterlies on wet days with the air originating from the Coral Sea (Figures 7(g) and 8(e)). This suggests that rainfall occurs inland in the vicinity of NP as a result of a moisture flux from the northeast and not from the adjacent Indian Ocean, which is geographically closer.

The results discussed above imply that, while the diurnal cycle of convergence is important for the timing of rainfall (as convergence still occurs above MP, RF and NP in the model on dry days; Figure 10), the low-level flow governs whether it rains or not at NP and RF in particular and to a lesser extent at MP where precipitation is primarily from deep convection in the model.

7. Conclusions

The aims of this work were to evaluate the diurnal cycles of both the rainfall and circulation within ACCESS1.3, and then to find out whether the modelled rainfall was produced under the correct flow regime. This work has shown that:

- The climatological representations of rainfall and MSLP in the model have high spatial correlations with the observational fields (0.82 and 1.0, respectively); however, the model has a large dry bias over northwest Australia (10% to more than 50% less rainfall) and the MSLP is systematically too low by 1–2 hPa across northern Australia (leading to anomalous easterlies at low levels).
- The model initiates rain 3 to 6 h too early in the east and north of Australia; this is associated with the premature triggering of deep convection (a common problem in GCMs).
- The timing and location of nocturnal rainfall over northwest Australia is comparable between the model and CMORPH.
- The inland, nocturnal rainfall in northwest Australia corresponds with increased convergence overnight following a continental-wide reorganisation of the flow around the heat low, which is also seen in the observations.
- A westerly flow at low levels brings the necessary moisture for rainfall at the coast of northwest Australia; however, an anomalous southeasterly (weakened westerly) is present on days when rain is initiated relative to dry days, which does not agree with Berry *et al.* (2011).
- Over northwest Australia, moisture is transported at low levels from the Gulf of Carpentaria and the Coral Sea into the continental interior (northeasterly flow) to initiate rain, which agrees with Berry *et al.* (2011).

This study shows that the model is not able to represent the timing of convective rainfall over much of the north and east of the Australian continent. Nevertheless, over northwest Australia, the model is capable of representing both the nocturnal convergence and the necessary moisture transports for rainfall to occur. This may imply that other models of a similar resolution (such as those in the CMIP5 ensemble) are able to represent the same processes over northwest Australia. Therefore, as part of a continuing program of research, the latest CMIP ensemble (CMIP5, to which ACCESS1.3 is a contributing model) will be analysed in a similar way to the study presented here.

Acknowledgements

The authors would like to thank the Australian National Computational Infrastructure National Facility for providing the computational platform on which the ACCESS1.3 model was run and the ARC Centre of Excellence for Climate System Science for providing the model and data infrastructure. CMAP Precipitation data were provided by the NOAA/OAR/ESRL PSD, Boulder, Colorado, USA, from their web site at http://www.esrl.noaa.gov/psd/. Pluviograph and AWAP data were provided by the Australian Bureau of Meteorology, ERA-Interim data were provided by the European Centre For Medium-Range Weather Forecasts and the TRMM 3B42 rainfall data were provided by NASA Goddard Earth Sciences Data and Information Services Center. This work was funded by the Australian Research Council grant DP0985665, 'Rainfall over the Maritime Continent and Northern Australia'.

References

Allen SC. 1980. Observational characteristics of the low-level jet at Daly Waters during project Koorin. *Aust. Meteorol. Mag.* **28**: 47–56.

Arnup SJ, Reeder MJ. 2007. The diurnal and seasonal variation of the northern Australian dryline. *Mon. Weather Rev.* **135**: 2995–3008.

Arnup SJ, Reeder MJ. 2009. The structure and evolution of the northern Australian dryline. *Aust. Meteorol. Oceanogr. J.* **58**: 215–231.

Basu BK. 2007. Diurnal variation in precipitation over India during the summer monsoon season: Observed and model predicted. *Mon. Weather Rev.* **135**: 2155–2167.

Berry G, Reeder MJ, Jakob C. 2011. Physical mechanisms regulating summertime rainfall over Northwestern Australia. *J. Clim.* **24**: 3705–3717.

Best MJ, Pryor M, Clark DB, Rooney GG, Essery RLH, Ménard CB, Edwards JM, Hendry MA, Porson A, Gedney N, Mercado LM, Sitch S, Blyth E, Boucher O, Cox PM, Grimmond CSB, Harding RJ. 2011. The Joint UK Land Environment Simulator (JULES), model description. Part 1: Energy and water fluxes. *Geosci. Model Dev.* **4**: 677–699, doi: 10.5194/gmd-4-677-2011.

Betts AK, Jakob C. 2002a. Evaluation of the diurnal cycle of precipitation, surface thermodynamics, and surface fluxes in the ECMWF model using LBA data. *J. Geophys. Res.* **107**: LBA 12-1–12-8, doi: 10.1029/2001JD000427.

Betts AK, Jakob C. 2002b. Study of diurnal cycle of convective precipitation over Amazonia using a single column model. *J. Geophys. Res.* **107**: ACL 25-1–25-13, doi: 10.1029/2002JD002264.

Betts AK, Fuentes JD, Garstang M, Ball JH. 2002. Surface diurnal cycle and boundary layer structure over Rondonia during the rainy season. *J. Geophys. Res.* **107**: LBA 32-1–32-14, doi: 10.1029/2001JD000356.

Bonner WD. 1968. Climatology of the low-level jet. *Mon. Weather Rev.* **96**: 833–850.

Brook RR. 1985. The Koorin nocturnal low-level jet. *Boundary-Layer Meteorol.* **32**: 133–154.

Brown JR, Jakob C, Haynes JM. 2010. An evaluation of rainfall frequency and intensity over the Australian region in a global climate model. *J. Clim.* **23**: 6504–6525.

Dai A. 2006. Precipitation characteristics in eighteen coupled climate models. *J. Clim.* **19**: 4605–4630.

Dai A, Trenberth KE. 2004. The diurnal cycle and its depiction in the community climate system model. *J. Clim.* **17**: 930–951.

Dai A, Giorgi F, Trenberth KE. 1999. Observed and model-simulated diurnal cycles of precipitation over the contiguous United States. *J. Geophys. Res.* **104**: 6377–6402, doi: 10.1029/98JD02720.

Dai A, Lin X, Hsu K-L. 2007. The frequency, intensity, and the diurnal cycle of precipitation in surface and satellite observations over low- and mid-latitudes. *Clim. Dyn.* **29**: 727–744.

Dee DP, Uppala SM, Simmons AJ, Berrisford P, Poli P, Kobayashi S, Andrae U, Balmaseda MA, Balsamo G, Bauer P, Bechtold P, Beljaars ACM, van de Berg L, Bidlot J, Bormann N, Delsol C, Dragani R, Fuentes M, Geer AJ, Haimberger L, Healy SB, Hersbach H, Hólm EV, Isaksen L, Kållberg P, Köhler M, Matricardi M, McNally AP, Monge-Sanz BM, Morcrette J-J, Park BK, Peubey C, de Rosnay P, Tavolato C, Thépaut J-N, Vitart F. 2011. The ERA-Interim reanalysis: Configuration and performance of the data assimilation system. *Q. J. R. Meteorol. Soc.* **137**: 553–597.

Dirnmeyer PA, Cash BA, Kinter JL III, Jung T, Marx L, Satoh M, Stan C, Tomita H, Towers P, Wedi N, Achuthavarier D, Adams JM, Altshuler EL, Huang B, Jin EK. 2012. Simulating the diurnal cycle of rainfall in global climate models: Resolution versus parameterization. *Clim. Dyn.* **39**: 399–418.

Fiedler S, Schepanski K, Heinold B, Knippertz P, Tegen I. 2013. Climatology of nocturnal low-level jets over North Africa and implications for modeling mineral dust emissions. *J. Geophys. Res.* **118**: 6100–6121, doi: 10.1002/jgrd.50394.

Garcia-Carreras L, Marsham JH, Parker DJ, Bain CL, Milton S, Saci A, Salah-Ferroudj M, Ouchene B, Washington R. 2013. The impact of convective cold pool outflows on model biases in the Sahara. *Geophys. Res. Lett.* **40**: 1647–1652, doi: 10.1002/grl.50239.

Gates WL. 1992. AMIP: The atmospheric model intercomparison project. *Bull. Am. Meteorol. Soc.* **73**: 1962–1970.

Gates WL, Boyle JS, Covey C, Dease CG, Doutriaux CM, Drach RS, Florino M, Gleckler PJ, Hnilo JJ, Marlais SM, Phillips TJ, Potter GL, Santer BD, Sperber KR, Taylor KE, Williams DN. 1999. An overview of the results of the atmospheric model intercomparison project (AMIP I). *Bull. Am. Meteorol. Soc.* **80**: 29–55.

Hewitt HT, Copsey D, Culverwell ID, Harriss CM, Hill RSR, Keen AB, McLaren AJ, Hunke EC. 2011. Design and implementation of the infrastructure of HadGEM3: The next-generation Met Office climate modelling system. *Geosci. Model Dev.* **4**: 223–253.

James IN. 1994. *Introduction to Circulating Atmospheres*. Cambridge University Press: Cambridge, UK.

Jones DA, Wang W, Fawcett R. 2009. High-quality spatial climate data-sets for Australia. *Aust. Meteorol. Oceanogr. J.* **58**: 233–248.

Joyce RJ, Janowiak JE, Arkin PA, Xie P. 2004. CMORPH: A method that produces global precipitation estimates from microwave and infrared data at high spatial and temporal resolution. *J. Hydrometeorol.* **5**: 487–503.

Keenan TD, Carbone RE. 2008. Propagation and diurnal evolution of warm season cloudiness in the Australian and Maritime Continent region. *Mon. Weather Rev.* **136**: 973–994.

Kowalczyk EA, Wang YP, Law RM, Davies HL, McGregor JL, Abramowitz G. 2006. The CSIRO Atmosphere Biosphere Land Exchange (CABLE) Model for Use in Climate Models and as an Offline Model. Marine and Atmospheric Research paper 013. CSIRO: Clayton South, Australia. http://www.cmar.csiro.au/e-print/open/kowalczykea_2006a.pdf (accessed 25 January 2014).

Maidens A, Stratton RA. 2006. *'Unified model documentation paper 27: convection scheme'*. Technical report, version 7. UK Met Office: Exeter, UK.

Martin GM, Ringer MA, Pope VD, Jones A, Dearden C, Hinton TJ. 2006. The physical properties of the atmosphere in the New Hadley Centre Global Environmental Model (HadGEM1). Part I: Model description and global climatology. *J. Clim.* **19**: 1274–1301.

Mohr KI. 2004. Interannual, monthly, and regional variability in the wet season diurnal cycle of precipitation in sub-Saharan Africa. *J. Clim.* **17**: 2441–2453.

Mori S, Jun-Ichi H, Tauhid YI, Yamanaka M, Okamoto N, Murata F, Sakurai N, Hashiguchi H, Sribimawati T. 2004. Diurnal land–sea rainfall peak migration over Sumatera Island, Indonesian Maritime Continent, observed by TRMM satellite and intensive rawinsonde soundings. *Mon. Weather Rev.* **135**: 2021–2039.

Neale R, Slingo J. 2003. The Maritime Continent and its role in the global climate: A GCM study. *J. Clim.* **16**: 834–848.

Parker DJ, Burton RR, Diongue-Niang A, Felton M, Taylor CM, Thorncroft CD, Bessemoulin P, Tompkins AM. 2005. The diurnal cycle of the West African monsoon circulation. *Q. J. R. Meteorol. Soc.* **131**: 2839–2860.

Pitchford KL, London J. 1962. The low-level jet as related to nocturnal thunderstorms over Midwest United States. *J. Appl. Meteorol.* **1**: 43–47.

Poveda G, Mesa OJ, Salazar LF, Arias PA, Moreno HA, Vieira SC, Agudelo PA, Toro VG, Alvarez JF. 2005. The diurnal cycle of precipitation in the Tropical Andes of Colombia. *Mon. Weather Rev.* **133**: 228–240.

Racz Z, Smith RK. 1999. The dynamics of heat lows. *Q. J. R. Meteorol. Soc.* **125**: 225–252.

Spengler T, Reeder MJ, Smith RK. 2005. The dynamics of heat lows in simple background flows. *Q. J. R. Meteorol. Soc.* **19**: 3147–3165.

Stratton RA, Stirling AJ. 2011. Improving the diurnal cycle of convection in GCMs. *Q. J. R. Meteorol. Soc.* **138**: 1121–1134.

Taylor KE, Williamson D, Zwiers F. 2000. 'The sea surface temperature and sea-ice concentration boundary conditions of AMIP II simulations'. PCMDI Report 60. Lawrence Livermore National Laboratory: Livermore, CA. http://www-pcmdi.llnl.gov/publications/pdf/60.pdf (accessed 25 January 2014).

Uppala SM, Kållberg PW, Simmons AJ, Andrae U, Da Costa Bechtold VDC, Fiorino M, Gibson JK, Haseler J, Hernandez A, Kelley GA, Li X, Onogi K, Saarinen S, Sokka N, Allan RP, Andersson E, Arpe K, Balmaseda MA, Beljaars ACM, Van de Berg L, Bidlot J, Bormann N, Caires S, Chevallier F, Dethof A, Dragosavac M, Fisher M, Fuentes M, Hagemann S, Hólm EV, Hoskins BJ, Isaksen L, Janssen PAEM, Jenne R, McNally AP. 2005. The ERA-40 re-analysis. *Q. J. R. Meteorol. Soc.* **131**: 2961–3012.

Walters DN, Best MJ, Bushell AC, Copsey D, Edwards JM, Falloon PD, Harris CM, Lock AP, Manners JC, Morcrette CJ, Roberts MJ, Stratton RA, Webster S, Wilkinson JM, Willett MR, Boutle IA, Earnshaw PD, Hill PG, MacLachlan C, Martin GM, Moufouma-Okia W, Palmer MD. 2011. The Met Office Unified Model Global Atmosphere 3.0/3.1 and JULES Global Land 3.0/3.1 configurations. *Geosci. Model Dev.* **4**: 919–941.

Wilson DR, Bushell AC, Kerr-Munslow AM, Price D, Morcrette CJ. 2008a. PC2: A prognostic cloud fraction and condensation scheme. Part I: Scheme description. *Q. J. R. Meteorol. Soc.* **134**: 2093–2107.

Wilson DR, Bushell AC, Kerr-Munslow AM, Price D, Morcrette CJ, Bodas-Salcedo A. 2008b. PC2: A prognostic cloud fraction and condensation scheme. Part II: Results of climate model simulations. *Q. J. R. Meteorol. Soc.* **134**: 2109–2125.

Xie P, Arkin PA. 1997. Global precipitation: A 17-year monthly analysis based on gauge observations, satellite measurements and numerical model outputs. *Bull. Am. Meteorol. Soc.* **78**: 2539–2558.

Yang G-Y, Slingo J. 2001. The diurnal cycle in the tropics. *Mon. Weather Rev.* **129**: 784–801.

Yang S, Smith EA. 2006. Mechanisms for diurnal variability of global tropical rainfall observed from TRMM. *J. Clim.* **19**: 5190–5226.

Yuan W, Yu R, Zhang M, Lin W, Chen H, Li J. 2012. Regimes of diurnal variation of summer rainfall over subtropical East Asia. *J. Clim.* **25**: 3307–3320.

